



# Effect of Aerated Pore Distribution on Bubble Plume Movement in a Cylindrical Aerated Tank

WAN TIAN<sup>1\*</sup>, YAN XINGXING<sup>1</sup>, CHENG WEN<sup>1</sup>, REN JIEHUI<sup>1</sup>, WANG MIN<sup>1</sup>, MENG TING<sup>1</sup>, LEI LEI<sup>1</sup>, FU RAN<sup>1</sup>, YANG KUN<sup>2</sup>

<sup>1</sup>Department of Municipal and environmental engineering, Faculty of Water Resources and Hydroelectric Engineering, State Key Laboratory Base of Eco-hydraulic Engineering in Arid Area, Xi'an University of Technology, Shaanxi, China

<sup>2</sup>Shanghai National Engineering Research Center of Urban Water Resources Co.Ltd, Shanghai, China

**Abstract:** *Aeration is crucial for biological wastewater treatment process but energy intensive. Aerated pore distribution in an aeration tank can control oxygen transfer and energy consumption. Therefore, this study aimed at elucidating the fundamental flow structure of gas phase in bubble plumes in a cylindrical tank with different aerated pore distance (ranged from 0.03-0.09m). Both experiments and numerical simulation were used. PIV (Particle Image velocimetry) technology was used for getting bubble phase flow field. Bubble population behavior model (BPBM) coupled with computational fluid dynamics (CFD) was established for numerical simulation. Results showed that aeration distances greatly affected the movement of gas-phase. When the aeration distances were large or small, the attractive interaction generated by air columns in different aeration pore caused a turbulence of bubble plume. At the meanwhile, a large of bubbles separated from the main air columns, which resulted in an unsteady gas-phase structure. The structure of bubble plume was relatively stable with an aerator spacing of 0.0625m in this study, which was beneficial for the connection between gas-phase and liquid-phase.*

**Keywords:** *Bubble plume; PIV; BPBM-CFD model; aerator pore distances; oxygen transfer*

## 1. Introduction

Aeration is crucial in wastewater biological treatment, which greatly affects the performance of biological process, and thus the wastewater treatment efficiency and operating cost [1, 2]. Pollutants in wastewater are biodegraded by microorganisms in biological reactors, and the oxygen is needed for the growth and metabolism of microorganisms [3]. Aeration, an energy consumption process which is generated by mechanical agitation, is used to supply oxygen for maintaining the microbial activity for well biodegradation [4]. Therefore, the urgent requirements from high efficiency and low consumption and the maximization trend of the reactors puts forward the new demand on aeration reactor optimal design [5, 6]. The efficiency of aeration reactors depends on the steady flow state of bubble plume inside, because the movement of bubble plume can directly affect the contact and mixing of the phases in the flow field. The mass and heat transfer efficiency of reactors can also be affected by the flow field and then expand the influence to the efficiency and consumption of the reactors. In conclusion, deeply exploring with the bubble plume structure hydro-mechanical behavior can help us to obtain helpful results for the further theoretical research and the optimal design of aeration reactor, which is significant for the increasingly serious problem of energy shortage and environmental pollution. It has been reported that aerators pore distance determined the uniformity of air inflation, and an appropriate aerator pore distribution created suitable bubble plume and through which control oxygen transfer and energy consumption in an aerator tank [7, 8]. Therefore, study on the effect of aerators pore distances on bubble plume movement behavior and oxygen transfer is of significant importance for wastewater treatment process.

\*email: [wantian@xaut.edu.cn](mailto:wantian@xaut.edu.cn)

Particle Image velocimetry (PIV) technology is one of the most feasible approaches for distinguishing bubble plume movement behaviors [9]. Introducing of the modern information processing algorithms to PIV for multiphase flow can improve the measurement performance, which is not only for the correct tracking of particles but also in spatio-temporal resolution [10]. By the applications to the study of aeration reactor, the velocity field information benefits engineers for improved design in energy efficiency [11, 12].

Therefore, this study aimed at elucidating the fundamental flow structure of dispersed gas phase in bubble plumes as a laboratory model of aeration process in a cylindrical tank. Both experiments and numerical simulation were used for investigating the bubble plume movement. We have developed a pre-processing algorithm for bubble-phase identification in complex two-phase images, and applied PIV for bubble phase. The data of spatio-temporal three-dimensional bubble velocity distribution were analyzed to discuss the relationship between the local and bulk aeration efficiency. In particular, this paper focused on the two-phase fluid dynamics read from the measurement data and its impact to the oxygen mass transfer. Bubble population behavior model (BPBM) coupled with computational fluid dynamics (CFD) was established for calculating the velocity flow of bubble plume. Oxygen transfer efficiency, which is related to the bubble plume movement, was evaluated to understand the correlation between the present result and previously obtained reactor's data [13, 14].

## 2. Materials and methods

### 2.1 Experimental Setup

The experimental set-up of the reactor was shown in Figure 1. A cylindrical tank with 700mm in height and 250mm in inner diameter was used for main body of the reactor. A rectangular tank had the height of 800mm and a square cross-section with the side of 280mm was used for water jacket surrounding the cylindrical tank to eliminate optical distortion of bubble images. According to our previous study, the air-blowing array on a circular tray was placed on the bottom where 24 holes were provided circumferentially around a central injector with the radii of 0.0417, 0.0625, and 0.0833m, respectively [14]. Air was evenly supplied by capillary tubes at a controlled pressure. Room temperature and atmospheric pressure acted on the model tank. A CCD camera (HG-100K, American Redlake Company) at 1000 fps in frame rate was used to record the behavior and structures of the bubble plumes. The type of camera lens was Nikkor lens with 60mm/2.8D, which produced by Nikon Company.

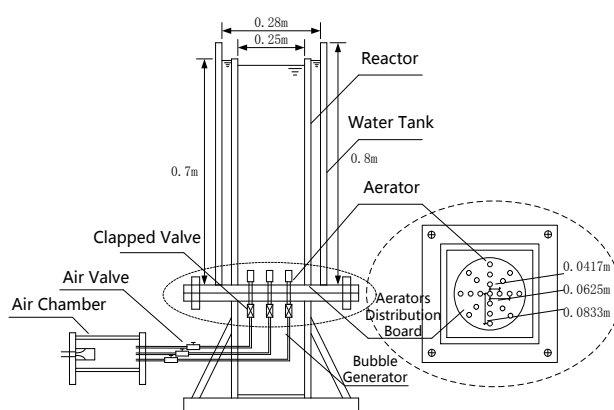


**Figure 1** Experimental set-up of aeration tank

In this study, tap water with the density of  $1.00 \times 10^3 \text{ kg/m}^3$  and kinematic viscosity of  $10^{-6} \text{ m}^2/\text{s}$  was used as the liquid phase in the aeration tank. Room air of laboratory with the density of  $1.28 \text{ kg/m}^3$  inflated into aeration tank by an air compressor was considered as the gas phase. The experimental conditions were showed in Table 1, and the parameters considered were according to our previous studies [8, 14].  $Q$  was the gas volume flow rate inflated by air compressor (ZB-0.12/7, Shanghai

Machinery Manufacturing Co. LTD).  $D$  was the distance of aerated pores in the circular tray as shown in Figure 1.  $H/W$  was the aspect ratio of the reactor.

**Table 1** The experiment conditions

No.	Q [ $10^{-5} \text{ m}^3/\text{s}$ ]	D [m]	H W[-]	P [KPa]
1	2.08	0.0417	1.5	7.0
2	2.08	0.0625	1.5	7.0
3	2.08	0.0833	1.5	7.0

## 2.2 Flow Measurement Method

The image acquisition system for PIV was shown in Figure 2. For high-quality bubble imaging, two optical set-ups were employed. One was used to cover the back side of the set up with a layer of vegetable parchment, which provided uniform diffused light inside the container and so that reflection of light at individual bubble interface became isotropic. Another was to fix two light sources at far distance in symmetrical coordinates for considering the brilliant light scattering angle of bubbles in the whole flow field to be measured.

In order to get accurate data, images taken by CCD were pre-processed for de-noised and post-processing. The original images were de-noised by Wave Transform Analysis [15-17]. Otsu's method [18] was adopted to determine the optimal threshold of the de-noised images. After threshold segmentation, the images were binarized by a program written by C++ language.

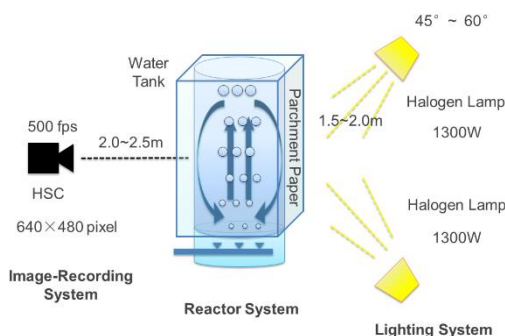


**Figure 2.** PIV image acquisition systems

## 2.3 Numerical Simulation

Based on the fluid mechanics theory, and considering gas-liquid two phase flow field reaction, coalescence and breakage of bubbles, a BPBM-CFD coupling calculation model were set up. The control equations of CFD were based on Euler/Euler mode [8]. The essence of BPBM model was to establish the conservation relations for dispersed phase (bubbles), which was shown in equation 1.

$$S(X, R, t) = B_C(X, R, t) - D_C(X, R, t) + B_B(X, R, t) - D_B(X, R, t) \quad (1)$$

In the equation,  $S(X, R, t)$  meant the net production rate of bubbles.  $B_C(X, R, t)$  meant the production rate of bubble coalescence, and  $D_C(X, R, t)$  meant the dissolved rate of bubble coalescence.  $B_B(X, R, t)$  meant the production rate of bubble broken, and  $D_B(X, R, t)$  meant the dissolved rate of bubble broken [19].

The dissolve of BPBM discrete equation considered the interacted force of bubbles, including drag force, virtual mass force, and wall shear stress [20, 21]. Therefore, when BPBM model had been written to Fluent UDF, it could supply the bubbles interacted forces and the process of bubble coalescence and broken. The CFD supplied the flow field parameters for the BPBM model calculation, such as the velocity of gas phase and liquid phase, gas volume fraction, turbulent kinetic energy and



pressure distribution. Then the simulation of gas-liquid two phase flow field could be accurately obtained by the BPBM-CFD coupling model.

The sizes of the reactor for numerical simulation were set in accordance with the physic model in experiments. The geometry was a vertical cylindrical tube with a pipe diameter of 250 mm and aeration volume flow rate of  $2.08 \times 10^{-5} \text{ m}^3/\text{s}$ , different aerator spacing distances ranged from 0.03 to 0.09m were set. Tri/Pace hawks grid cell was used for meshing on the bottom of the reactor and the air outlet of aeration. The meshing number is 613311. According to our previous study, air inlet at the bottom of the reactor was set as the velocity inlet boundary conditions, and the top export was set as the pressure outlet boundary conditions [14]. The aeration holes at the bottom and the reactor wall were set as nonslip wall boundary condition.

## 2.4 Oxygen Transfer Efficiency

The momentum equations and turbulence equations were the second order discrete formats. The volume fraction was set as Quick discrete format, and phase-coupled simple method was used for the coupling of pressure and speed coupling. The time step of numerical simulation was 0.001s. Dissolved oxygen testing apparatus (HQ40-d, American HACH Corporation) was used for dissolved oxygen concentration in each experimental condition.

Oxygen transfer efficiency was an important evaluation index to evaluate the dynamic efficiency of the aerating device. The ability of filling oxygen referred to amount of oxygen transfer into water in per unit time at standard state (1atm, 20°C). The ability of filling oxygen was calculated from the following equation [22].

$$OC = K_L a \times C_s \times V \quad (2)$$

where:

OC -- Oxygenation Capacity, (mg/h),

$K_L a$  -- Oxygen Transfer Coefficient, (1/h)

$V$  -- Volume of Reservoir, ( $\text{m}^3$ ),

$C_s$  -- Dissolved Oxygen Saturation Concentration, (mg/L).

The  $K_L a$  was referred at the temperature of 20°C by using equation 3[23].

$$K_L a_{(20)} = K_L a_{(T)} \times 1.024^{T-20} \quad (3)$$

The oxygen transfer efficiency ( $E_A$ ) refers to the percent of amount of oxygen transferred into liquid in total oxygen supply by aeration system. The equation was as following equation [24].

$$E_A = \frac{K_L a_{(20)} \times C_s \times V}{N \times Q} \quad (4)$$

where:

$E_A$  -- Oxygen Transfer Efficiency (%),

$N$  -- Oxygen Coefficient ( $\text{kg}/\text{m}^3$ ),

$Q$  -- Aeration volume flow rates [ $\text{m}^3/\text{s}$ ].

## 3. Results and discussions

### 3.1 Bubble plume structure and flow field

In the physical model research, the bubble plume temporal-spatial distribution in the aerated reservoir was measured by the PIV system. The characteristics and velocity distribution of flow field were particularly analyzed. Bubble plume flow field at the different aerated pore distances were

showed in Figure 3. Clearly, the aerated pore distance greatly affected the bubble plume movement structure. When the aerated pore distance was small (0.0417 m), the bubble injection area was concentrated relatively. The whole bubble plume form shrank because that the plume columns were inter-attracted when bubbles raised from the bottom to the upper. The shearing action by liquid phase increased with the continue rising of bubble plume, and the bubble plume began to spread out to form a movement structure with a shrinkage bottom and diffused upper part. Under this condition, the bubble plume formed a spiral structure with a narrow and tiny amplitude swing cycle. The bubble plume movement had a greatly change with an increasing aerator pore distance. Under the distance of 0.0833m, the bubble plume structure was stable at the bottom and there were no attraction effects among plume columns. Bubbles nearly straight rose from the bottom to the top of the reactor, and the bubble plume mixture and liquid turbulence were not obvious. In the upper part of the bubble columns, a large number of bubbles were free out. This condition caused a relatively short stay time of bubbles in reactor, which was not benefit for oxygen transfer. When the aerator pore distances were 0.0625 m, the bubble plumes in the flow field were well-distributed. Bubble plumes in the bottom of flow field stably rose up with a helical form. The swings of bubble plume in the aerator were periodical and steady at the bottom of the flow field. Finally, the plume columns mixed in the upper part of the reactor and resulted in a heavy liquid turbulence, which was benefit for enhancing the contact time and contact area between bubbles and water.

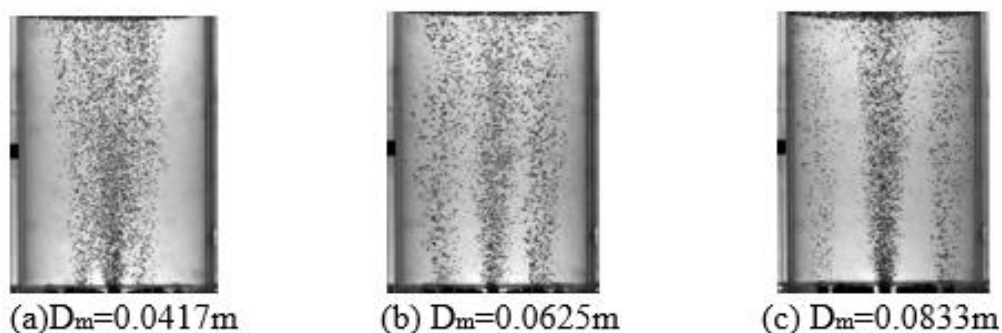


**Figure 3.** Bubble plume flow fields at aerated pore distance: (a) 0.0417m, (b) 0.0625m, and (c) 0.0833m

The time-dependent and time-average bubble flow velocity fields of bubble plume were shown in Figures 4 & 5, respectively. Clearly, the concentration of aerated pore distance caused the shrinkage of gas areas in flow field. When the aerated pore distance was 0.0417m, the highest velocity was about 0.36m/s, which appeared in the bottom of the flow field. When the distance increased to 0.0625m, the flow field of gas phase was uniform and the average velocity was about 0.35m/s. As the distance became larger, the flow field distribution of gas phase was dispersive, and the highest velocity was 0.38m/s in the bottom area of gas column. The gas columns concentrated by attractive interaction, and therefore reduced the swing of bubble plume. The dispersing aerated pores resulted in the relatively independent movement of bubble plume columns. Several “Non-bubble areas” between columns were found in this condition, which might greatly affect the oxygen mass transfer efficiency in biological treatment reactor.

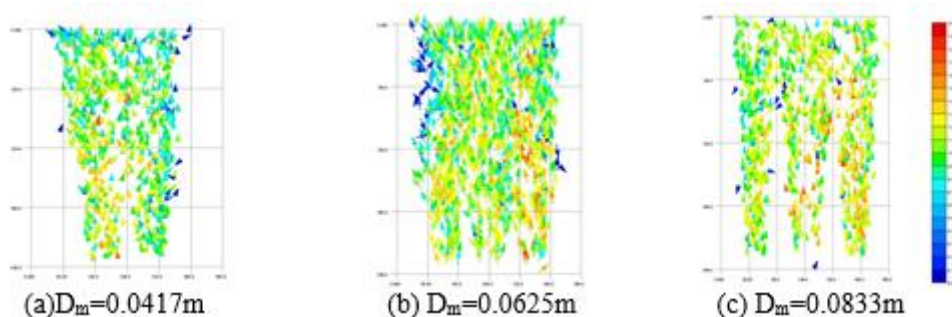


**Figure 4.** Time-dependent bubble flow velocity field at aerated pore distance of 0.0417m; 0.0625m and 0.0833m

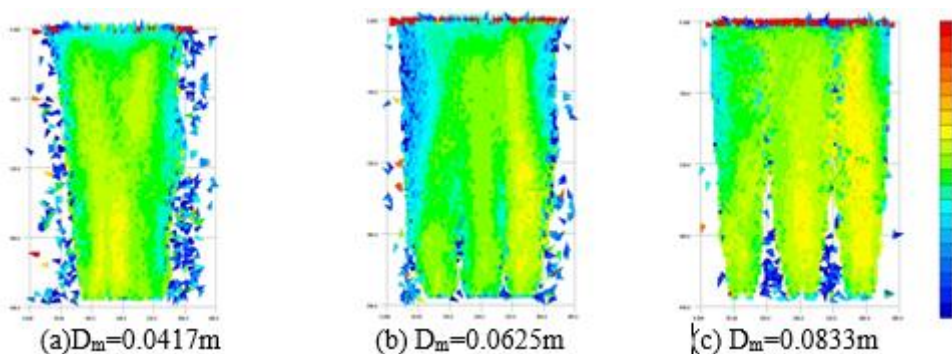


**Figure 5.** Time-average bubble flow velocity field at aerated pore distance of 0.0417m; 0.0625m and 0.0833m

### 3.2 Bubble plume flow field by numerical simulation

#### 3.2.1 Verification of numerical simulation

Numerical simulation of bubble plume flow field was also conducted in this research. The aeration conditions in numerical simulation were set in accordance with the physic model in experiments. The bubble plume flow fields were obtained by experiments and numerical simulation, as seen in **Figure 6**. Clearly, the gas-phase velocity distribution obtained by numerical simulation had a good agree with by PIV experiments. The trend of flow fields were with accordance. The radial velocity distributions of gas meet the index law. The maximum value of velocity appeared in the center of the column, which was in line with the actual situation. Therefore, the BPBM-CFD model could accurately simulate the movement of bubble plume.

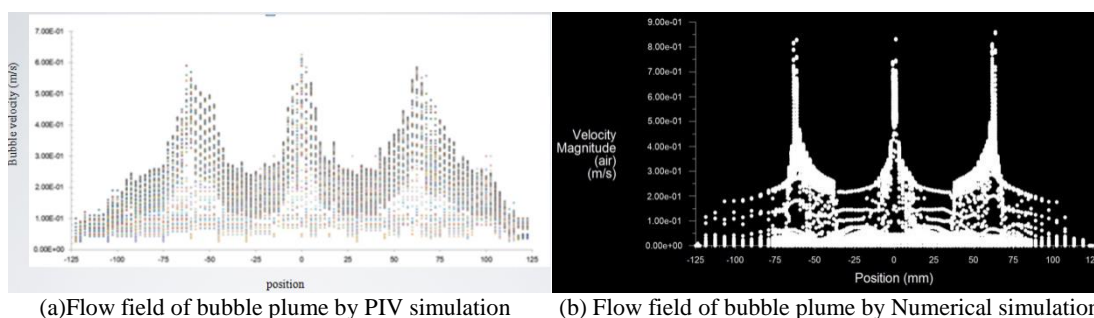


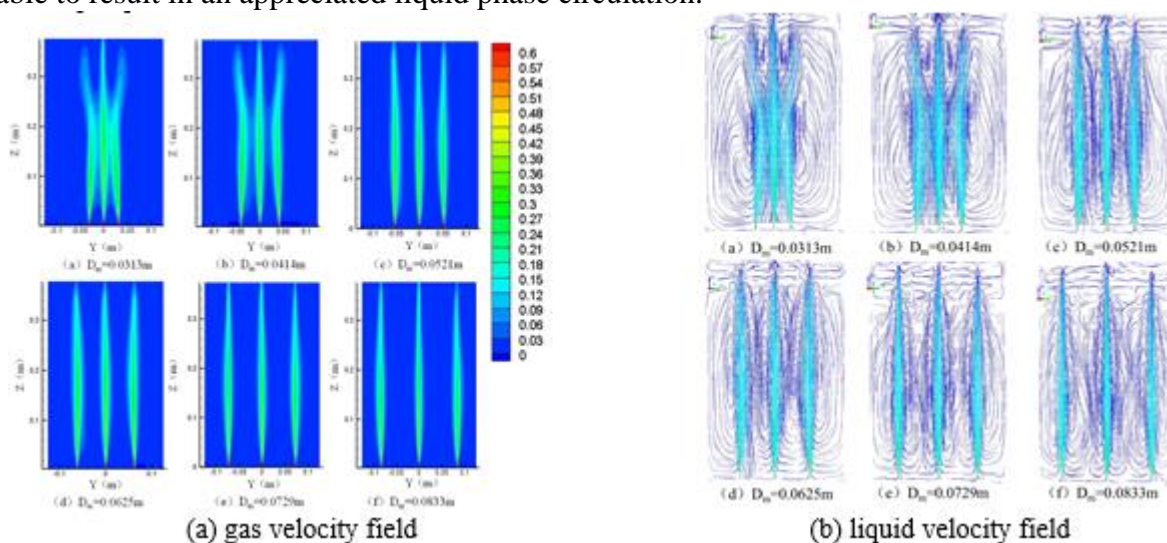
**Figure 6.** The instantaneous gas velocity field contrast by experiment and numerical simulation ( $Q=2.08 \times 10^{-5} \text{m}^3/\text{s}$ ,  $H/W=1.5$ )

#### 3.2.2 Gas- liquid two phase flow field in aeration tank

The instantaneous gas velocity and liquid flow field in X-radial section of aeration tank can be seen in Figure 7. The velocity of gas phase was similar with the gas flow field distribution obtained by PIV

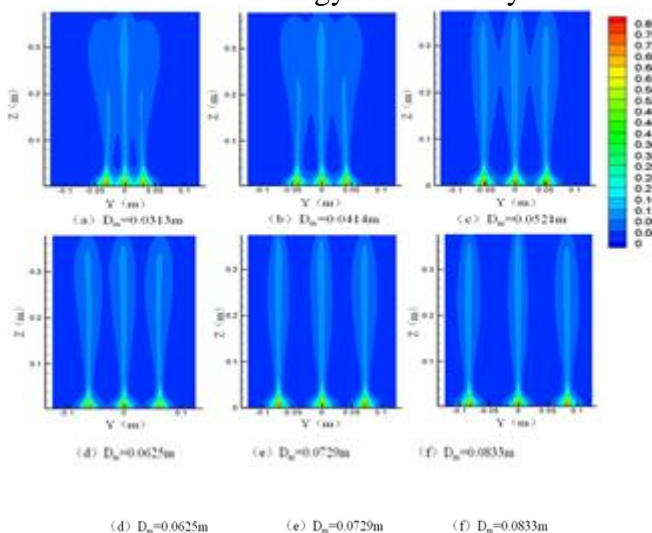
experiments. The change trend of gas phase velocity distribution was similar with different aerated pore distances. With the increase of aerated pore distance, the attractive interaction caused by gas phase movement reduced. When the aerated pore distance was too large or too small, the gas column swung unsteady and a large number of bubbles dispersed from the main gas columns because of the attractive interaction among columns or the side walls of reactor, which resulted in an unsteady structure of gas phase. A modest distribution of aerated pore could get a stable gas movement structure, which was beneficial for the contact between gas phase and liquid phase.

For the liquid phase flow field, the concentrated aerated pore distance caused increasing liquid movement, and the hydraulic dead zone decreased. However, the velocity gradient of liquid phase resulted from the rising gas movement, and therefore the liquid phase was not circled. With larger distance of aerated pore in reactor, the liquid phase flow field began to form velocity partition because of different velocity gradients by the rising of gas columns. The liquid phase flow direction at the half bottom flow field was similar with the rising up direction of gas phase. At the upper half part of the flow field, gas phase formed downward velocity when arriving at the free surface, which was also unable to result in an appreciated liquid phase circulation.



**Figure 7.** The instantaneous gas velocity and liquid two-phase flow field in X-radial section.

Aerated pore distances greatly impacted the bubble plume movement and velocity flow field of liquid phase. In order to illustrate the effect of aerated pore distances on flow field, the liquid turbulence energy and turbulence viscosity were analyzed as shown in Figure 8. Obviously, the aerated pore distances greatly affected the turbulence energy and viscosity.



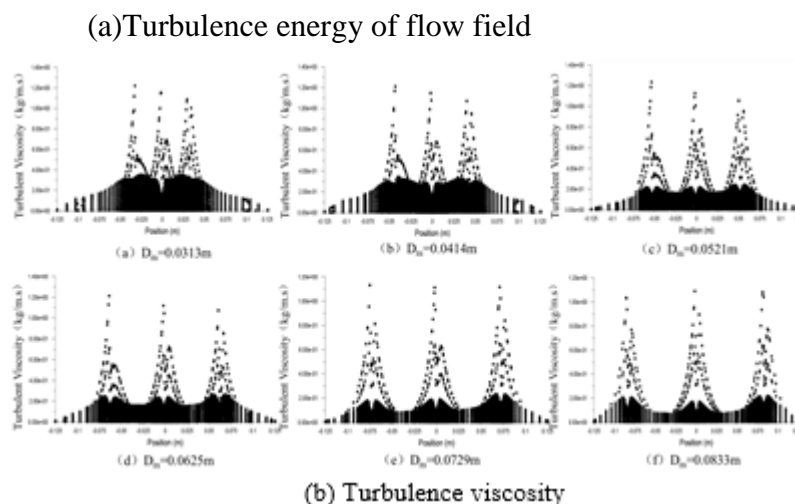


**Figure 8.** Effect of the aerated pore distance on the turbulence energy and viscosity of the whole flow field

### 3.3 Oxygen transfer in aeration tank

According to the study results obtained above, different aerator pore distances caused the changes on flow field velocity distribution and liquid turbulence, which determined the contact time and contact area between air and water and thus the oxygen transfer as well. Therefore, oxygen transfer parameters, oxygen transfer coefficient ( $K_{La}$ ) and oxygen transfer efficiency ( $E_A$ ) were calculated to describe the relationships among aerated pore distances and  $K_{La}$ ,  $E_A$ , respectively. Figure 9 showed the results.

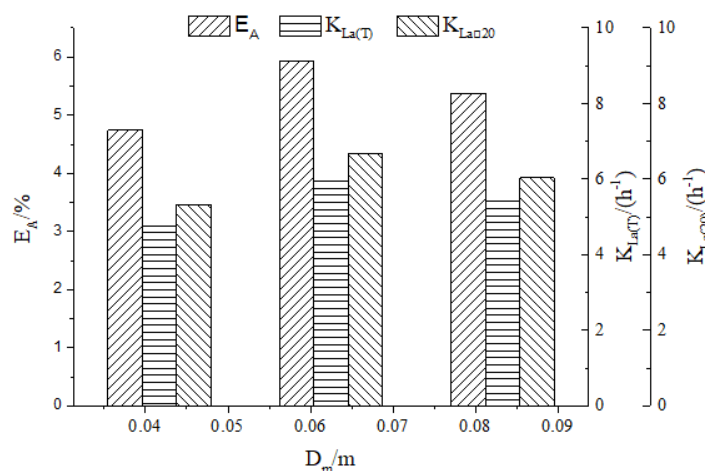


**Figure 9.** The result of rinsing aeration under different aerator pore distances ( $Q = 2.08 \times 10^{-5} \text{ m}^3/\text{s}$  cm  $H/W=1.5$ ,  $C_s=10\text{mg/L}$ )

Clearly, an appreciated aerated pore distribution was important for oxygen transfer. Too large or small pore distance could result in a relative lower oxygen transfer coefficient. The trend of  $E_A$  will vary inversely with  $K_{La}$ . The aerated pore distribution mainly affected the bubble plume movement structure during aeration process. According to the flow field we obtained above, the attractive interactions among bubble plume columns were obvious when the distance was small, and the movement area of gas phase concentrated on the center of the liquid phase flow field. Therefore, the contact areas between bubbles and liquid phase were unable to increase effectively. At the meanwhile, the unsteady gas phase velocity distribution (Figures 4-7) resulted in unevenly dissolved oxygen concentration distribution in the liquid phase. The center of the liquid phase might be rich in oxygen



and other area might be ‘oxygen-deficit’, which greatly affected the oxygen transfer rate. Unsteady bubble plume structure caused strong turbulence of liquid phase, which increased the probability of collision and merger among bubbles [24]. Therefore, the contact time and contact areas of gas and liquid phase decreased, resulted in lower oxygen transfer efficiency. For larger aerator pore distance, bubble plume in the flow field was dispersive, and the interaction among bubble columns was low. The bubble plume rose almost vertically during ascent, which caused relative weak turbulence for liquid phase and a large number of bubbles were quickly diffused from the main bubble plume columns. Thus the oxygen transfer efficiency was relative lower. For an appreciated aerated pore distance, bubble plume distributed unevenly in the flow field. The slight attractive interaction among bubble plume columns was beneficial for the formation of stable liquid circulation at the upper of the flow field. The contact time and contact areas increased, and the velocity of gas phase in flow field was equal-distributed, which was helpful for the increase of oxygen transfer efficiency.

#### 4. Conclusions

According to the above analysis of experimental results and numerical simulation, the following main conclusions are obtained.

(1) PIV experiments results showed that the temporal-spatial distribution of bubble plume varies with changes of aerated pore distance. When the aerator pore distance was 0.0625m, the flow field was well-distributed that steady liquid circulation and turbulent fluctuation were formed. The velocity distribution of gas-phase was uniform. When the aerated pore distance was 0.0417m, 0.0625m and 0.0833m, the highest velocity of each condition was 0.36m/s, 0.35m/s and 0.38m/s, respectively.

(2) The BPBM-CFD model can accurately simulate the movement of bubble plume, and the gas-phase flow field distribution obtained by numerical simulation had a good agree with by PIV experiment. Numerical simulation results showed that the aerated pore distances greatly affected the liquid phase velocity distribution, and too large or small pore distances could not bring uniform liquid velocity distribution and even increased energy consumption.

(3) Results of oxygen transfer efficiency showed that increase of aerator pore distances led to a nonlinear change to the  $K_{La}$  and  $E_A$ , and an appropriate aerator pore distribution will be important to improve the operating efficiency of aeration reactor.

**Acknowledgments:** The authors would like to acknowledge the financial support from the National Science Foundation of China (Grant: 51679192 & NFSC 51709224) and Postdoctoral Science Foundation of Shannxi Province (Grant: 2017BSYDZZ63).

#### References

1. MALDONADO, S.L., RASCH, D., KASJANO, A., BOUWES, D., KRÜHNE, U., KRULL, R., Multiphase microreactors with intensification of oxygen mass transfer rate and mixing performance for bioprocess development. *Biochem. Eng. J.*, **139**(15), 2018, 57-67.
2. MCCLURE, D., KAVANAGH, M., FLETCHER, F., BARTON, W., Oxygen transfer in bubble columns at industrially relevant superficial velocities: experimental work and CFD modeling. *Chem. Eng. J.*, **280**, 2015, 138-146.
3. WANG, H., VERDUGO, A. S., SUN J., WANG, J., YANG, Y., JIMÉNEZ, F. H., Experimental study of bubble dynamics and flow transition recognition in a fluidized bed with wet particles. *Chem. Eng. Sci.*, **211**(16), 2020, *in press*.
4. ZHOU, X., MA, Y., LIU, M., ZHANG, Y., CFD-PBM simulations on hydrodynamics and gas-liquid mass transfer in a gas-liquid-solid circulating fluidized bed. *Power Tech.*, **362**(15), 2020, 57-74.
5. PINO-HERRERA, D.O., FAYOLLE, Y., PAGEOT, S., HUGUENOT, D., ESPOSITO G., HULLEBUSCH, E. D., PECHAUD Y., Gas-liquid oxygen transfer in aerated and agitated slurry systems with high solid volume fractions. *Chem. Eng. J.*, **350**, 2018, 1073-1083.
6. WEITBRECHT, V., SEOL, D., PIV measurements in environmental flows: Recent experiences at



- the Institute for Hydromechanics in Karlsruhe. *J. Hydro. Environ.*, **5**, 2011, 231-245.
- 7.CHENG, Y., TORREGROSA, M., VILLEGAS, A., DIEZ, F. J., Time resolved scanning PIV measurements at fine scales in a turbulent jet. *Int. J. Heat. Fluid. Flow.*, **32**, 2011, 708-718.
- 8.BUZOIANU, D.A., PANAITESCU, C., BOMBOS, M., STOICA, M. E., Study on efficiency increasing of biological stage by sequential operating of aeration reactors, *Revista De Chimie*, 67(5), 2016, 962-966
- 9.CIRLIORU, T.M., CIOCAN, C.D., BARRE, S., DJERIDI, H., PANAITESCU, V., Quadrant analysis of turbulent mixing layer, *Revista De Chimie*, 64(3), 2013, 326-329
- 10.FERNANDA, H., CHARLES, L., ZHANG, H., Influence of bubble plumes on evaporation from non-stratified waters. *J. Hydro.*, **438**, 2012, 84-96.
- 11.RAJESH, K. U., HARISH, J. P., SHANTANU, R., Liquid flow patterns in rectangular air-water bubble column investigated with Radioactive Particle Tracking. *Chem. Eng. Sci.*, **7**(96), 2013, 152-164.
- 12.POURTOUSI, M., SAHU, J. N., GANESAN, P. Effect of interfacial forces and turbulence models on predicting flow pattern inside the bubble column. *Chem. Eng. Process.*, **75**, 2014, 38-47.
- 13.CHENG, W., HU, B. The velocity field of multiphase flow and efficiency of biological aeration filter. *J. Hydro.*, **2**(22), 2010, 260-264.
- 14.CHENG, W., LIU H., WANG, M., WANG, M., The effect of bubble plume on oxygen transfer for moving bed biofilm reactor. *J. Hydro. Seri. B.*, **26**(4), 2014, 664-667.
- 15.XUE, T., WANG, Q. F., LIU, X. W., Bubble image processing based on ARM in gas-liquid two-phase flow. *Adv. Mater. Res.*, **694-697**, 2013, 2630-2633.
- 16.CERQUEIRA, R.F.L., PALADINO, E.E., YNUMARU, B.K., Image processing techniques for measurement of two-phase bubbly pipe flows using particle image and tracking velocimetry(PIV/PTV), *Chem. Eng. Sci.*, **189**, 2018, 1-23.
- 17.MURGAN, I., BUNEA, F., CIOCAN, G. D., Experimental PIV and LIF characterization of a bubble column flow, *Flow Meas. Instrum.*, **54**, 2017, 224-235.
- 18.QU, J., MURAI, Y., YAMAMOTO, F., Simultaneous PIV/PTV measurements of bubble and particle phases in gas-liquid two-phase flow based on image separation and reconstruction. *J. Hydro.*, **16** (6), 2004, 756-766.
- 19.LIAO, Y.X., LUCAS, D., A literature review of theoretical models for drop and bubble breakup in turbulent dispersions, *Chem. Eng. Sci.*, **64**(15), 2009, 3389-3406.
- 20.CHEN, Y.J., DING, J., WENG, P.F., LU, Z.B., LI X.W., A theoretical model describing bubble deformability and its effect on binary breakup in turbulent dispersions, *Eur. J. Mech. B-Fluid*, **75**, 2019, 352-360.
- 21.BESBES, S., EL HAJEM, M., BEN AISSIA, H., CHAMPAGNE, J.Y., JAY, J., PIV measurements and Eulerian-Lagrangian simulations of the unsteady gas-liquid flow in a needle sparger rectangular bubble column, *Chem. Eng. Sci.*, **126**, 2015, 560-572.
- 22.LARS, B., Next steps in clean water oxygen transfer testing- A critical review of current standards. *Water Res.*, **157**, 2019, 415-434.
- 23.CAPODICCI, M., CORSINO, S. F., TRAPANI, D. D., TORREGROSSA, M., VIVIANI, G., Effect of biomass features on oxygen transfer in conventional activated sludge and membrane bioreactor systems, *J. Clean. Prod.*, **240**, 2019, 118071.
- 24.HERRMANN-HEBER, R., REINECKE, S.F., HAMPEL, U., Dynamic aeration for improved oxygen mass transfer in the wastewater treatment process., *Chem. Eng. J.*, **386**, 2020, 122068

Manuscript received: 01.06.2020